ACS OMEGA

Open Access



http://pubs.acs.org/journal/acsodf

Article

# Voltametric Sensor Based on Magnetic Chitosan Acetylindole-Based Nanocomposite for the Determination of Sulfamethazine

Mohamed Abd-Elsabour,* Mortaga M. Abou-Krisha, Abdulrahman G. Alhamzani, Abdullah N. Alotaibi, and Tarek A. Yousef

Cite This: *ACS Omega* 2024, 9, 17323−17333

Read Online

ACCESS | Metrics & More | Article Recommendations | Supporting Information

**ABSTRACT:** Sulfamethazine (SMZ), a persistent antibiotic, is frequently detected in drinking water and milk. For this reason, our research aimed to develop a novel electrochemical sensor based on a magnetic nanocomposite supported on chitosan modified by 3-acetylindole through the formation of chitosan acetylindole Schiff base (Chs-Aci). The objective was to detect extremely low concentrations of SMZ in milk. The synthesized nanocomposites were characterized by various techniques, including FT-IR, XRD, EDX, SEM, and TEM. To enhance the electrocatalytic efficiency for sensitive SMZ detection in food samples, a magnetic chitosan acetylindole nanocomposite (M-Chs-Aci) was employed as a modifier for a carbon paste electrode (CPE). The electrochemical measurements revealed that the M-Chs-Aci/CPE exhibits good electrocatalytic performance compared to a bare CPE. Moreover, low detection limit, repeatability, and stability were achieved at 0.021 $\mu$M, 3.83%, and 94.87%, respectively. Finally, the proposed M-Chs-Aci/CPE proved to be highly effective in detecting SMZ in milk samples. The obtained findings paved the way for the effective usability of M-Chs-Aci/CPE as a sensor for detecting SMZ in real samples, with acceptable recoveries of 95%−98.87%.

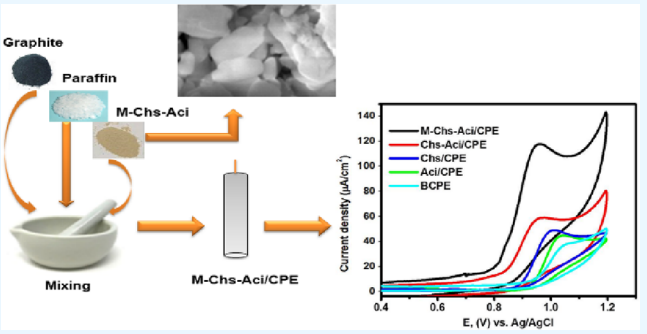


## 1. INTRODUCTION

The widespread prevalence of pathogenic microorganisms has led to the emergence of numerous fatal diseases that pose a threat to human health. Consequently, researchers are actively exploring new functional materials with high biomedical activity. Sulfa-medicines (sulfonamides) are widely used as antibacterial agents for treating many infectious diseases. Particularly, sulfamethazine (SMZ) is a sulfa medication with high antibacterial effectiveness that is frequently recommended for the therapeutic treatments of livestock illnesses, including gastrointestinal infections and respiratory tract infections, as well as growth supplements.[1,2] However, the excessive use of SMZ can contaminate food and drinking water, posing potential risks to human health. Therefore, there is a pressing need to develop precise methods for the sensitive detection of SMZ in food and environmental samples, which requires significant research efforts.

In recent years, several methods have been employed for detecting sulfonamides and their derivatives, such as electrophoresis[3,4] and various chromatographic methods.[5−9] Although these methods are effective and offer the required limit of detection, their main disadvantages include uneconomical measurements. As a result, researchers have increasingly focused on developing novel electrochemical devices due to their advantageous characteristics, including rapid analysis, excellent sensitivity, enhanced selectivity, lower cost, and lower limits of detection (LOD).[10−12] A set of modified electrodes for electrochemical detection of SMZ have been reported, including gold electrodes improved by multiwalled carbon nanotubes and/or graphene oxide nanoribbons,[13] glassy carbon electrodes (GCEs) modified with graphene oxides coated with the core−shell of a Cu−Ag composite, gold nanoparticles, and/or strontium niobium composite,[14−16] a GCE in the form of a network of graphite-nitride nanosheets modified with strontium tungstate nanospheres,[17] and cerium vanadate anchored to multiwalled carbon nanotubes as a modifier for a GCE.[18] Each approach exhibits its own sensitivity, selectivity, and detection limits while also facing specific interferences and challenges. To achieve more accurate and rapid quantification of SMZ at frequently encountered levels in diverse natural samples, the design of superior electrochemically based sensors remains crucial. Recently, there has been a revolution in the development of new voltametric sensors with desirable features such as portability and ease of fabrication.

Received: December 26, 2023
Revised: March 8, 2024
Accepted: March 22, 2024
Published: April 4, 2024

**Scheme 1. Scheme of Chs-Aci Schiff Base Preparation and Synthesis of M-Chs-Aci Composite by Magnetite Eco-Precipitation on Chs-Aci Schiff Base**

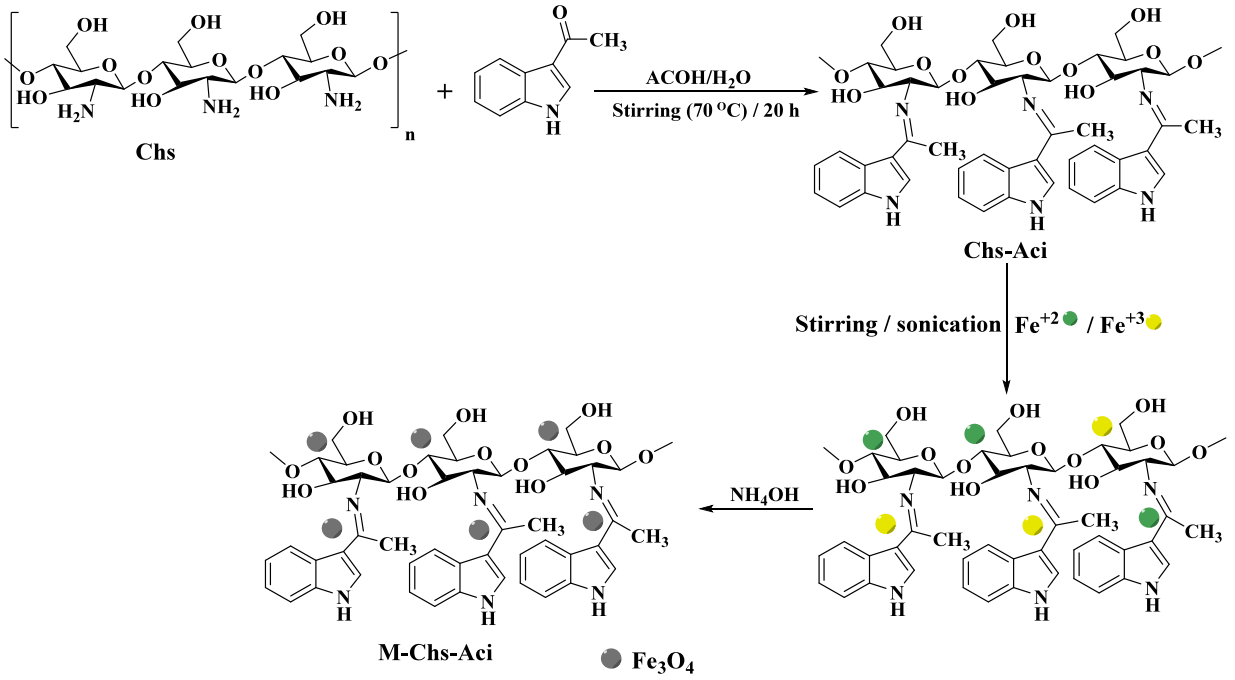


In this context, carbon paste electrodes (CPEs) have gained widespread use due to their excellent biocompatibility, safety, cost-effectiveness, reproducibility, and consistent performance. Throughout analytical chemistry, CPEs have been frequently employed as voltametric sensors for various electrochemical investigations.[19,20] Regarding modified CPEs, differential pulse voltammetry (DPV) has been applied to achieve low limits of detection. The development and utilization of modified electrodes have garnered significant interest in improving the sensitivity and selectivity of electrochemical measurements for many important bioactive compounds.[21] In this regard, chitosan (Chs) is a biopolymer derived from the deacetylation of readily available chitin. It can be utilized in a wide scale of applications, including food, medicine, cosmetics, and water treatment based on its appealing characteristics such as mechanical strength, nontoxicity, biodegradability, and biocompatibility.[22] Chs is considered a bifunctional agent. This property was attributed to it containing amino and hydroxyl groups as active groups. This enables its interaction with various reactive materials containing electrophilic or nucleophilic groups, leading to the formation of stable covalent-based materials.[23]

Several recent studies have demonstrated the effective utilization of Chs in the production of electrochemical sensors.[24,25] Chs exhibits significant swelling in water and is soluble under acidic conditions, which can impact sensor stability.[26] Consequently, researchers have been actively working to enhance the mechanical and stability features of Chs-based sensors.[27] Functionalizing Chs by reacting it with active groups, such as −OH and/or -$NH_2$, has proven to be an efficient route for improving the stability of Chs-based sensors.[28] Notably, the reaction involving the amino group enables the production of a new Schiff base structure.[29] This approach has shed light on the preparation of a 3-acetylindole-Chs Schiff base for the first time. Additionally, $Fe_3O_4$ nanoparticles, known for their high catalytic efficiency and surface activity, have been incorporated as fillers to enhance the mechanical and electrical conductivities of the Schiff base. This aids in improving the sensor stability and sensitivity for the electrochemical determination of SMZ.[30,31]

It should be noted that no literature has yet referenced the use of this modified electrode for the voltametric determination of SMZ. Thus, we prepared a magnetic 3-acetylindole-chitosan Schiff base as a modifier for the CPE, creating a simple, rapid, sensitive, and cost-effective electrochemical sensor for SMZ detection. This research has resulted in the design of an electrochemical sensor for SMZ detection, offering enhanced features, such as easy electrode preparation, a broad linear range, high selectivity, low detection limits, rapid regeneration, and good stability. The details and discussions regarding these advancements are described below.

## 2. MATERIALS AND METHODS

**2.1. Materials and Solutions.** Chitosan (DD = 95%, MW: 100,000−300,000 D), 3-acetylindole (purity ≥96%), ferrous sulfateheptahydrate ($FeSO_4.7H_2O$, purity ≥98%), ferric chloride hexahydrate ($FeCl_3.6H_2O$, purity ≥97%), ammonia solution (25%), acetic acid (≥99%), and ethanol (≥99%) were supplied from Sigma-Aldrich. SMZ ($C_{12}H_{13}N_4O_2SNa$, purity ≥98%) was delivered from Supelco Analytical Products (Germany). Graphite powder, sodium hydroxide, monosodium phosphate, and disodium phosphate were procured from El-Nasr Pharmaceutical Chemicals (Egypt). All solutions were freshly prepared by using ultrapure water (18.2 MΩ·$cm^{-1}$) at 25 °C. A phosphate-buffered solution (PBS) of 0.1 M $NaH_2PO_4$−$Na_2HPO_4$ (pH 7.0) was used as the supporting electrolyte. The SMZ stock solution was prepared daily by dissolving an exact amount of SMZ in PBS.

**2.2. Apparatus and Instrumentation.** Fourier transform of infrared spectroscopy (FT-IR) spectra of the present M-Chs-Aci nanocomposites were measured from 4000 to 400



https://doi.org/10.1021/acsomega.3c10390
ACS Omega 2024, 9, 17323−17333

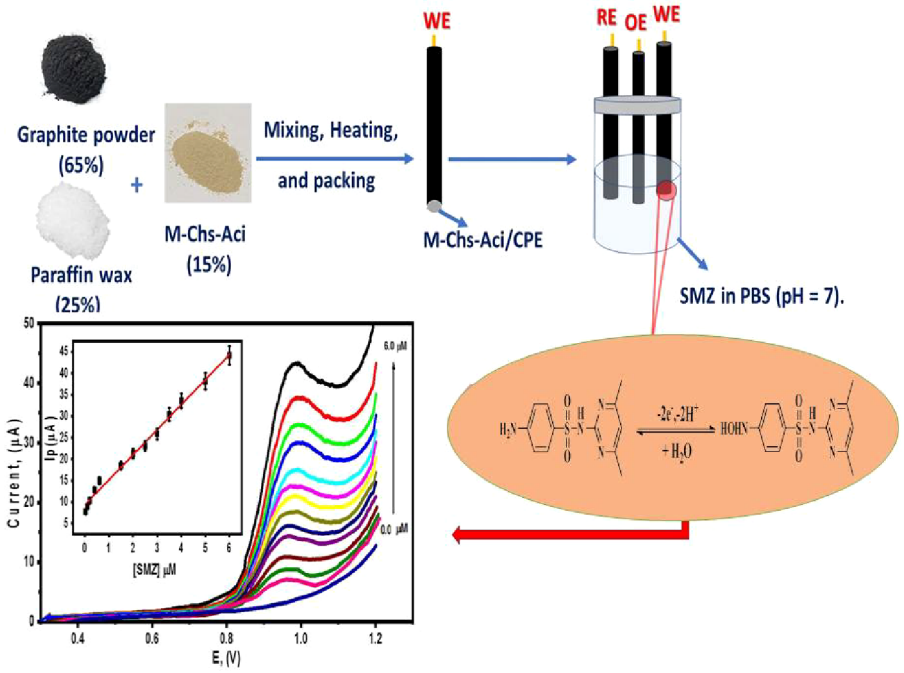


**Figure 1.** Graphical abstract of the preparation of the M-Chs-Aci/CPE.

$cm^{-1}$ using the KBr pellets method with an FT-IR spectrometer (Model 8400 S, Shimadzu, Japan). The samples were pressed into tiny disks and mixed with KBr for FTIR measurements. X-ray diffraction (XRD) data of the synthesized nanocomposites were obtained by utilizing diffractometer instruments (Bruker D-8, Germany), equipped by CuK$\alpha$ X-ray sources with a wavelength of 0.15406 nm. The data were collected in the range of $2\theta = 5°$ to 80° with a scan rate2°/min. Besides, surface morphology and elemental analyses of the nanocomposite microstructures were inspected via scanning electron microscopy (SEM) (JEOL, model JSM-IT200, Japan). Energy-dispersive X-ray spectroscopy (EDXS) data were performed to examine the chemical compositions of the M-Chs-Aci nanocomposites as an attached unit to JEOL (model JSM-IT200, Japan) with 30 kV as the accelerating voltage, 1.0 nA probing current, and 10 mm working distance. Moreover, transmission electron microscopy (TEM) was employed to analyze the particle size and investigate the morphological characteristics of the prepared samples using (JEOL/JEM-F200, Japan) at 200 kV as the accelerating voltage and a resolution of 0.23 nm. The voltametric measurements were quantified using a Potentiostat (263, EG-G-PARC). The employed electrochemical cell comprised of three types of electrodes: platinum wire (Model K0266), Ag/AgCl electrode (Model K0265), and M-Chs-Aci/CPE, which were used as auxiliary, reference , and working electrodes, respectively. All measurements were carried out at room temperature.

**2.3. Preparation of the Schiff Base (Chitosan-3-Acetylindole).** Chs (1.0 g) was added to 100 mL of an aqueous solution of acetic acid (2.0%) and stirred for 10 min at room temperature. Then, 3-acetylindole (0.4 g, 0.0025 M) was added to the suspension solution, and the mixture was stirred at 70 °C for 20 h. The resulting mixture was then poured into a Petri dish and allowed to evaporate the solvent. The obtained precipitate was washed several times with ethanol and dried in a vacuum oven at 60 °C overnight, resulting in the formation of the final product.

**2.4. Preparation of Nanocomposite (Magnetite/chitosan-3-Acetylindole).** Similar to the method used for the preparation of the chitosan/$Fe_3O_4$ nanocomposite.[32] The magnetite/chitosan-3-acetylindole nanocomposite was synthesized using a coprecipitation approach, as depicted in Scheme 1. Initially, a 100 mL suspension solution of chitosan-3-acetylindole (1.0 g) and $Fe^{2+}/Fe^{3+}$ (at a molar ratio of 1:2) was stirred for 4.0 h. Subsequently, the solution was subjected to ultrasonication for 15 min at 100 °C. Gradually, an equivalent volume of ammonia solution (20%) was added to obtain the nanocomposite. The resulting black precipitate was separated using a permanent magnet and washed with distilled water until neutralization. Finally, the product was dried in an oven at 70 °C for 24 h.

**2.5. Preparation of Different Working Electrodes.** A set of working electrodes was prepared for this study, including a bare carbon paste electrode (BCPE), a chitosan-3-acetylindole-modified carbon paste electrode (Chs-Aci/CPE), and a magnetite-chitosan-3-acetylindole-modified carbon paste electrode (M-Chs-Aci/CPE). The M-Chs-Aci/CPE working electrode was fabricated by manually combining pure graphite powder, paraffin wax, and M-Chs-Aci in a ratio of 60:25:15% w/w) using an agate mortar and pestle. This specific ratio was chosen based on the better current intensities observed in the supplementary data (Figure 1S). The resulting homogeneous pastes were packed into glass tube tips and connected to the cell by using copper wires. Similarly, the Chs-Aci/CPE and BCPE working electrodes were prepared by replacing M-Chs-Aci with Chs-Aci in the case of Chs-Aci/CPE (Scheme 1), and using only graphite and wax in a ratio of 75:25% (w/w) for BCPE. The synthesized electrode surfaces were then polished until they became shiny and activated through repeated cyclic voltammetry (CV) in phosphate buffer solution (PBS) with a pH of 3.2, between 0 and 1.0 V, until steady voltammograms were obtained. A fresh surface was created by extruding more paste from the tip and manually polishing it on clean paper to achieve a smooth surface.Figure 1



https://doi.org/10.1021/acsomega.3c10390
ACS Omega 2024, 9, 17323−17333

**2.6. Determination of SMZ in Milk Sample.** To determine the concentration of SMZ in milk samples obtained from a local market, a standard addition method was employed. A 5 mL milk sample was mixed with 10 mL of $CH_3CN$ to eliminate any protein traces present. The resulting mixtures were then centrifuged at 6000 rpm for 40 min. Subsequently, the supernatant was purified by using a 0.45 $\mu$m nylon membrane filter before being transferred to the electrochemical cell. Aliquot of SMZ were added to the purified supernatant, followed by dilution with PBS (pH = 7.0) to achieve the desired SMZ concentrations for analysis using the proposed electrochemical method.

## 3. RESULTS AND DISCUSSION

**3.1. Structural Characterization of Samples.** *3.1.1. Vibrational Analysis.* The utilization of infrared spectroscopy to examine the network structure of the synthesized samples is widely recognized as a valuable contribution. In this study, we employed FTIR (Fourier transform infrared) spectroscopy to investigate the macrostructure of the samples. Figure 2a

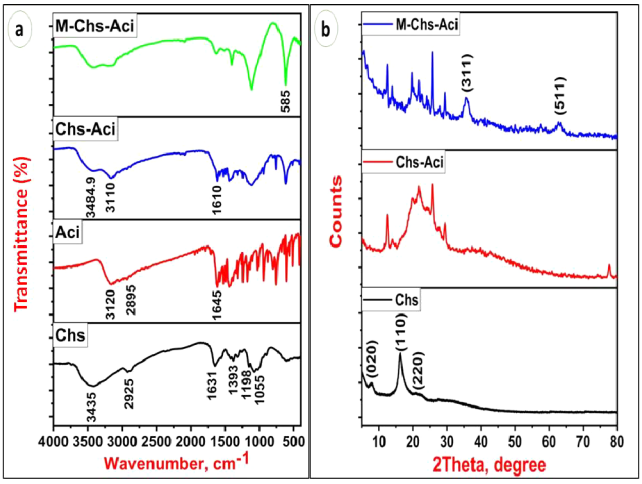


**Figure 2.** (**a**) FTIR of Chs, Aci, (Chs-Aci) Schiff base, and (M-Chs-Aci) nanocomposite and (**b**) XRD of Chs, (Chs-Aci) Schiff base, and (M-Chs-Aci) nanocomposite.

demonstrates the FT-IR spectra of chitosan (Chs), 3-actylindole (Aci), Schiff base (Chs-Aci), and nanocomposite (M-Chs-Aci). As detected from Figure 2a, for the Chs spectra, the broad band at 3435 $cm^{-1}$ is due to the stretching vibration of the −OH and $-NH_2$ (hydroxyl and amine) groups. The bands at about 2925 and 1393 $cm^{-1}$ are assigned as vibrations (stretching and bending) of the the aliphatic−CH group, respectively. The bending vibrations of the primary amine ($NH_2$) group appeared at 1631 $cm^{-1}$. The bands located at 1198 and 1055 $cm^{-1}$ are correlated to asymmetric stretching vibrations of the glycoside linkage (C−O−C) between units of Chs and (C−O−C) of the pyranose amine ring, respectively.[33] Meanwhile, the FT-IR spectrum of Aci is also presented in Figure 2a, revealing characteristic bands at 3120 and 2895 $cm^{-1}$ for aromatic and aliphatic −CH groups, respectively. Additionally, a band at 1645 $cm^{-1}$ corresponds to the carbonyl group.[34]

The interaction between Chs and ACi, resulting in the formation of the Chs-Aci Schiff base, was confirmed by the blue FTIR spectra presented in Figure 2a. The spectral changes observed in the blue spectra, compared to the spectra of Chs and ACi, indicate the successful formation of the Schiff base. Notably, the disappearance of the band at 1631 $cm^{-1}$ in the FTIR spectra of Chs-Aci, in comparison with Chs, further confirms the reaction between Chs and ACi. This reaction leads to the formation of an imine group, which exhibits a characteristic band at1610 $cm^{-1}$.[35] The broad band observed at 3484.9 $cm^{-1}$ can be attributed to the stretching vibrations of the hydroxyl groups. Additionally, the characteristic band at 3110 $cm^{-1}$ corresponds to the aromatic −CH group of the indole ring. These bands in the Schiff base spectra indicate that ACi has been successfully grafted onto the Chs backbone.

Also, the FT-IR spectra of the magnetic nanocomposite (M-Chs-Aci) are represented by green color, as shown in Figure 2a. In this spectrum, new bands are observed along with shifts in the position of certain bands, confirming the formation of a new network backbone. A comparison between Chs-Aci and the nanocomposite revealed slight shifts in the characteristic bands associated with imine and hydroxyl groups. This can be attributed to the overlapping of the polar groups of Chs with $Fe_3O_4$. Additionally, the intensity of the main characteristic bands in the nanocomposite spectrum (M-Chs-Aci) decreases with the addition of magnetite. Furthermore, the (M-Chs-Aci) spectra exhibit a band at 585 $cm^{-1}$, which is assigned to the Fe−O group, indicating the presence of magnetic $Fe_3O_4$ supported on the (Chs-Aci) Schiff base.[36]

*3.1.2. XRD Patterns.* X-ray diffraction (XRD) spectra are an effective technique for characterizing the prepared samples. In Figure 2b, the XRD patterns of the samples are presented, with Chs represented by the black pattern, the Schiff base by the red pattern, and the nanocomposite by the blue pattern. The XRD pattern of the Chs sample displayed diffraction peaks at 7.86°, 16.34°, and 19.9°, showing the semicrystallinity nature of Chs polymer.[37] Additionally, the purity of Chs was confirmed by the absence of any other diffraction peaks associated with impurities. The XRD pattern of the Chs-Aci Schiff base (red pattern) demonstrated new peaks correlated to 3-acetylindole at 12.36, 13.94, 21.8, 25.76, and 29.4°, beside clear changing of characteristic diffraction peaks of Chs that confirmed the condensation of Chs with 3-acetylindole resulting in the Chs-Aci Schiff base, as shown in Figure 2b.

Moreover, the XRD pattern of the M-Chs-Aci nanocomposite, blue pattern in Figure 2b, exhibits two distinctive diffraction peaks at $2\theta$ = 35.5° and 62.8°. These two bragg's peaks are related to cubic $Fe_3O_4$NPs,[38] as well as they correspond to Miller indices of (311) and (511), respectively. In addition, the average crystalline size ($D$) of $Fe_3O_4$NPs was computed by the XRD pattern data of two Bragg's peaks at (311) and (511) using the famous Debye−Scherrer formula:

$$D = \frac{0{\cdot}94\lambda}{\beta \cos \theta} \quad (1)$$

where $\lambda$ is the radiation wavelength and $\beta$ is the full width at half-maximum (fwhm). The average crystalline size of $Fe_3O_4$NPs in the nanocomposite sample was found to be around 14 nm.

*3.1.3. Morphological Analysis.* The morphological structure of the M-Chs-Aci nanocomposite was examined by SEM, as illustrated in Figure 3a. The SEM image of the M-Chs-Aci nanocomposite showed clear nanosheet-like structures. Furthermore, the surface exhibited uneveness, roughness, and contained pores that provided suitable binding sites for the target molecules, driving to a higher electrocatalytic activity.


https://doi.org/10.1021/acsomega.3c10390
ACS Omega 2024, 9, 17323−17333

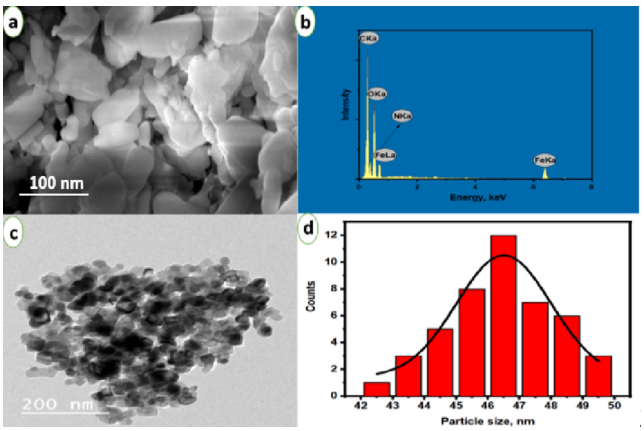


**Figure 3.** (a) SEM image, (b) EDX profile, (c) TEM image, and (d) particle size distribution of the M-Chs-Aci nanocomposite.

To study the elemental analysis of the samples' composition, an energy dispersive X-ray spectrum (EDS) was utilized. The EDX profile for the nanocomposite sample is illustrated in Figure 3b. The intense signal of the C element is obviously observed to suggest that carbon is the predominant element in the nanocomposite. In addition, the signature of the oxygen element is also detected. The presence of a nitrogen element signal in the EDX spectrum was also pinned and related to Aci, which exhibits successful condensation between Chs and Aci. The signal of iron element was also clearly observed, confirming the presence of $Fe_3O_4$, and revealed the successful formation of the nanocomposite. The absence of any other signals of any impurity indicates the high purity of the obtained nanocomposite. The transmission electron spectroscopy (TEM) image of the M-Chs-Aci nanocomposite is presented in Figure 3c. The image revealed a smaller and compact core−shell structure, which comprises dark-colored ellipsoidal and spherical-shaped particles of $Fe_3O_4$ NPs and the light contrast matrix of Chs-Aci Schiff base. Additionally, from the particle size distribution curve, the average size of nanocomposite was provided to be 46.5 nm (Figure 3d).

**3.2. Electrochemical Characterization of Various Electrodes.** The electrochemical behaviors of the CPE (BCPE), improved CPE by Schiff base (Chs-Aci/CPE), and modified CPE by nanocomposite (M-Chs-Aci/CPE) were examined by cyclic voltammograms (CVs) in 0.1 M KCl comprising1.0 mM of $[Fe(CN)_6]^{3-/4-}$ at a scan rate of 50 mV/s, as shown in Figure 4. It is clear that the surface of all applied working electrodes revealed reversible redox reactions with separation peak potentials ($\Delta E_p$) of 0.96 0.64, 0.63, 0.62, and 0.48 V for BCPE, Aci/CPE, Chs/CPE, Chs-Aci/CPE, and M-Chs-Aci/CPE, respectively. Moreover, compared with BCPE, the anodic current signals at Aci/CPE, Chs/CPE, Chs-Aci/CPE, and M-Chs-Aci/CPE are increased by 0.16 mA, 0.35 mA, 0.45 mA, and 0.77 mA, respectively. As shown, the working electrode M-Chs-Aci/CPE demonstrates the best results compared to other electrodes. Based on these results, it is clear that the Chs-Aci and M-Chs-Aci samples enhanced the voltammetric responses of the BCPE by facilitating charge transfer at the surfaces of the modified electrodes. The high electrocatalytic efficiency of M-Chs-Aci/CPE ensures that this sample is an appropriate candidate for analytical applications such as the determination of SMZ.

The active surface area ($A$) for the prepared electrodes was calculated by Randles−Sevcik eq [$I_p = (26.9 \times 10^4)\, n^{1.5} A\, D_R{}^{0.5} \upsilon^{1.5} Co$], where $D_R$ refers to the diffusion coefficients for ($[Fe(CN)_6]^{3-/4-}$; $D_R = 7.6 \times 10^{-6} cm^2 s^{-1}$), $I_p$ refers to the peak currents in amperes, and $n$ is the number of transferring charges during the electrochemical processes ($n$ = 1). The electroactive surface areas for BCPE, Aci/CPE, Chs/CPE, Chs-Aci/CPE, and M-Chs-Aci/CPE were 0.009 $cm^2$, 0.013 $cm^2$, 0.016 $cm^2$, 0.019 $cm^2$, and 0.034 $cm^2$, respectively, revealing a substantial increase (increased to 277%) in electroactive surface area of the M-Chs-Aci/CPE compared to the BCPE.

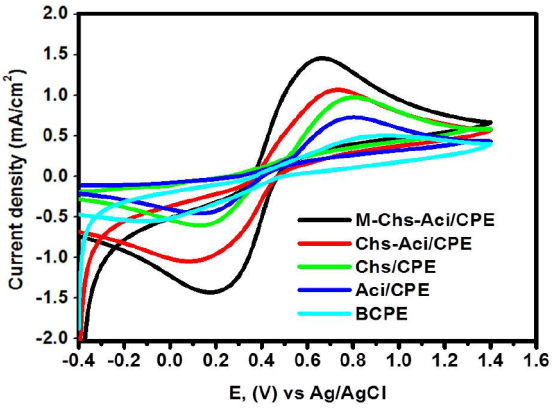


**Figure 4.** CVs of 1.0 mM of $[Fe(CN)_6]^{3-/4-}$ in 0.1 M KCl at a scan rate of 50 mV/s at BCPE, Aci/CPE, Chs/CPE, Chs-Aci/CPE, and M-Chs-Aci/CPE.

**3.3. Electrochemical Behavior of SMZ.** The electrochemical behaviors of (3.0 $\mu$M) of SMZ was examined via the CV method at different applied electrodes in PBS (pH = 7) at a scan rate of 50 mV/s, and in the potential range of 0.4−1.2 V (vs Ag/AgCl). The obtained results are shown in Figure 5. A

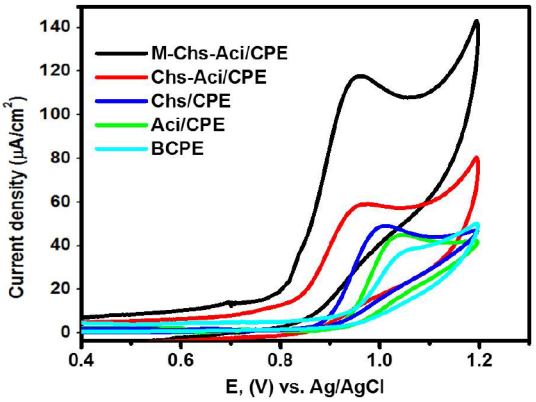


**Figure 5.** CVs of 3.0 $\mu$M of SMZ in 0.1 M of PBS (pH = 7.0) with a scan rate of 50 mV/s at BCPE, Aci/CPE, Chs/CPE, Chs-Aci/CPE, and M-Chs-Aci/CPE.

significant anodic peak of SMZ was observed at all electrodes and followed the order: BCPE< Aci/CPE < Chs/CPE < Chs-Aci/CPE < M-Chs-Aci/CPE. Moreover, no reductive peak was observed in the reverse scan for SMZ, proving the irreversible nature of SMZ oxidation, which is in good accordance with the reported literature.[39]

It is evident that the anodic peak currents of the BCPE were not distinctive. Interestingly, however, the anodic peak current signals are increased by 1.25, 1.375, 1.65, and 3.35 times at Aci/CPE, Chs/CPE, Chs-Aci/CPE, and M-Chs-Aci/CPE


https://doi.org/10.1021/acsomega.3c10390
ACS Omega 2024, 9, 17323−17333

surfaces compared with the BCPE. Moreover, the oxidative peaks at the Chs-Aci/CPE and M-Chs-Aci/CPE seem sharper than those of the Aci/CPE, Chs/CPE, and the BCPE with soft negative shifts in the anodic peak potential by 0.085 and 0.1 V at Chs-Aci/CPE and M-Chs-Aci/CPE, respectively. These results have been associated with the enhanced electroactive areas of Chs-Aci/CPE and M-Chs-Aci/CPE, which would facilitate efficient electron transferring. The electrode of the nanocomposite sample (M-Chs-Aci/CPE) exhibited the highest enhancement, suggesting that the M-Chs-Aci/CPE working electrode could be used to trace SMZ in real samples.

The enhanced electrocatalytic efficiency of the modified electrode is attributed to the introduction of Aci-functionalized Chs, which exhibits a more robust attachment to the electrode surface, thereby enhancing the electrode stability. Furthermore, the potent interactions between Aci-Chs and the functional groups of the SMZ, specifically, hydrogen bonding, electrostatic interaction, and $\pi-\pi$ interaction, are expected to enhance analyte adsorption on the electrode surface, thereby improving the determination sensitivity. On the other hand, the introduction of $Fe_3O_4$ nanoparticles as fillers into the structure of chitosan improves the electric conductivity as well as its mechanical properties. These nanoparticles display high surface reaction activity, large surface-to-volume ratio, high catalytic efficiency, and strong adsorption capability that can be helpful to attain enhanced stability and sensitivity of a sensor.[39−42]

**3.4. Effect of pH.** The effect of PBS pH on the oxidation peak of 3.0 $\mu$M SMZ is investigated using linear sweep voltammetry (LSV) within the pH range of 3.0−9.0 at a scan rate of 50 mV/s, as illustrated in Figure 6. It is observed that,

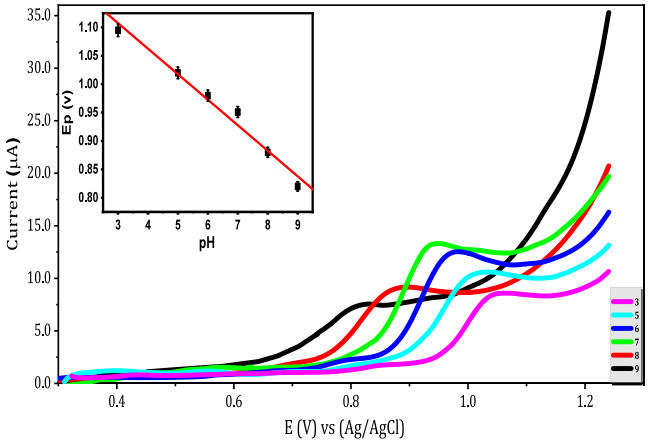


**Figure 6.** LSVs of 3.0 $\mu$M SMZ in 0.1 M PBS with various pH values for M-Chs-Aci/CPE at a scan rate of 50 mV/s. Inset part shows the dependence of $E_p$ on the pH value.

with further increasing the pH value, potential of the oxidation peak ($E_p$) shifts gradually toward more negative value, proving the involvement of $H^+$ in the SMZ oxidation process. The plots of $E_p$ vs pH values display a linear relationship that is described in the following equation:

$$E_p(\mathrm{v}) = 1.24\text{-}0.045\ \mathrm{pH}, \quad r^2 = 0.989 \tag{2}$$

the measured value (−0.045 V/pH) is comparable to the theoretical Nernstian value (−0.059 V/pH); thus, the oxidation process of SMZ involves an equal number of $H^+$ and electrons.[2] Moreover, the increment in pH values from 3.0 to 7.0, resulted in an increase in the peak current observed during the oxidation of SMZ, with the highest peak observed at pH 7.0. However, with a further increase in pH, a gradual decrease in the current signal was observed. This response is consistent with previous findings regarding the oxidation of SMZ at different pH values.[16] According to this study of pH values, the optimum pH value for the oxidation of SMZ using M-Chs-Aci/CPE is regarded as 7.0.

**3.5. Effect of Scan Rate.** To investigate the influence of the potential scan rate on the nature of the electrochemical oxidation process of SMZ at M-Chs-Aci/CPE, LSV for 3.0 M SMZ was used at various scanning rates ($\nu$) in 0.1 M PBS (pH = 7.0). The findings indicated that the potentials of the SMZ anodic peak were noticed shifting toward the positive value as the scan rate raised from 10 to 500 mV/s, as illustrated in Figure 7a. Furthermore, with increasing scan rates, the signal of the anodic current increases. However, as the scan rate was increased further to levels above 500 mV/s, distortion of the peak shape was observed, particularly at high SMZ concentration. Additionally, the linear relationship between $I_p$ and $\nu^{0.5}$ indicated that the SMZ oxidation process at the M-Chs-Aci/CPE surface is a diffusion-based behavior (eq 3), which is shown in the inset part of Figure 7a. Furthermore, the relationship between log ($I_p$) as the $Y$-axis and log ($\nu$) as the abscissa demonstrated that the SMZ oxidation is a diffusion-based process, as shown in Figure 7b. Such a relationship, which further follows Eq 4, gives a straight line. The value of the resulting slope was 0.4, which is extremely close to 0.5, and indicated the electron transfer coefficient ($\alpha$) for the diffusion-controlled process.[42]

The number of electrons involved in the SMZ oxidation process ($n$) was calculated by applying Laviron's equation (eq 5). As illustrated in Figure 7c, calculation of ($\alpha n$) value depended on the slope resulting from plotting $E_p$ vs log ($\nu$), which is used in Eq 6.

$$I_p\ (\mu\mathrm{A}) = 1.09 + 3.01\nu^{0.5}\ (\mathrm{mV/s})^{0.5}, \quad r^2 = 0.998 \tag{3}$$

$$\log\ (I_p)\ (\mu\mathrm{A}) = 0.38 + 0.40 \log\ (\nu)\ (\mathrm{mV/s})^{0.5}, \quad r^2 = 0.998 \tag{4}$$

$$\Delta I_p/\Delta \log\ (\nu) = 0.059\alpha n \tag{5}$$

$$E_p(V) = 0.87 + 0.066 \log\ (\nu)\ (\mathrm{mV/s}), \quad r^2 = 0.992 \tag{6}$$

the result of the calculation for $n$ was 1.78 ≈ 2. Therefore, the suggested mechanism for SMZ electrochemical oxidation can be expressed as shown in Scheme 2.

**3.6. Chronoamperometric Study.** The diffusion coefficient ($D$) value for SMZ voltammetric oxidation at the M-Chs-Aci/CPE was calculated according to the chronoamperometric approach using the following eq 7.

$$I_p = nFAD^{0.5}C\pi^{-0.5}t^{-0.5} \tag{7}$$

where $A$ is the geometric surface area of the M-Chs-Aci/CPE ($A$ = 0.12 $cm^2$), $C$ refers to the SMZ concentration (mM), and $t$ denotes the elapsed time (s). Figure 8 displays the chronoamperograms of different SMZ concentrations (0.08, 0.12, 0.15, 0.2, and 0.25 $\mu$M) at a constant potential of 0.96 V in PBS (pH = 7.0). For varied SMZ concentrations, the relationship between $I_p$ and $t^{-0.5}$ created straight lines. The diffusion coefficient was calculated to be 9.4 × $10^{-6}$$cm^2$/s.


https://doi.org/10.1021/acsomega.3c10390
ACS Omega 2024, 9, 17323−17333

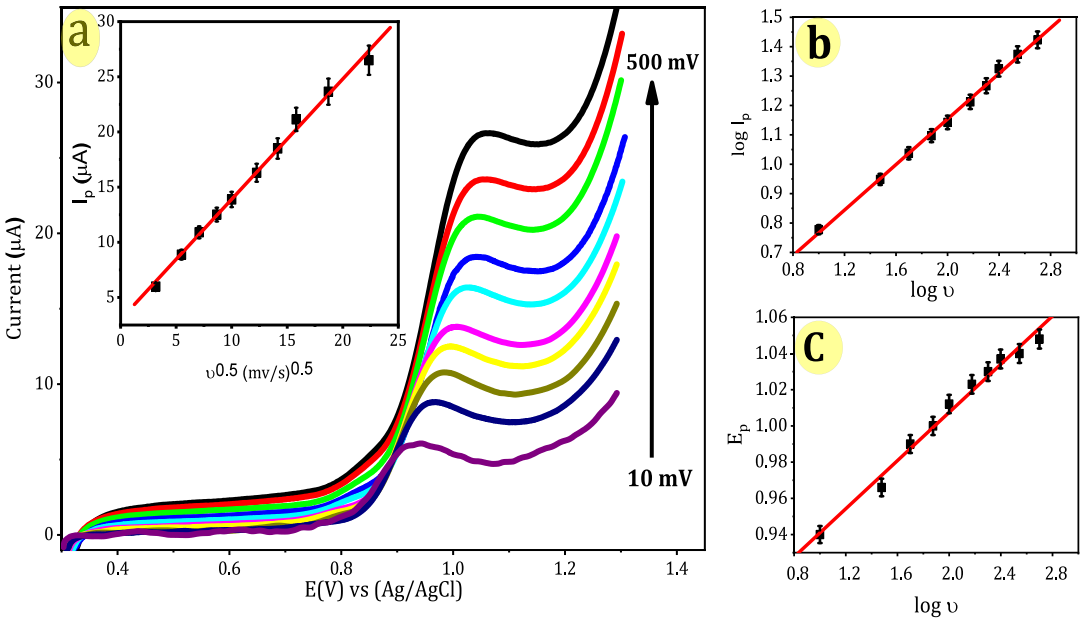


**Figure 7.** (a) LSVs of 3.0 $\mu$M SMZ in 0.1 M PBS (pH 7.0), at the M-Chs-Aci/CPE at various scan rates from 10 to 500 mV/s. The inset part displays the dependency of the current of the anodic peak on $v^{0.5}$, (b) plot of log ($I_p$) vs log ($v$), and (c) plot of ($E_p$) vs log ($v$).

**Scheme 2. Suggested Mechanism of Electro-Oxidation of SMZ at the M-Chs-Aci/CPE**

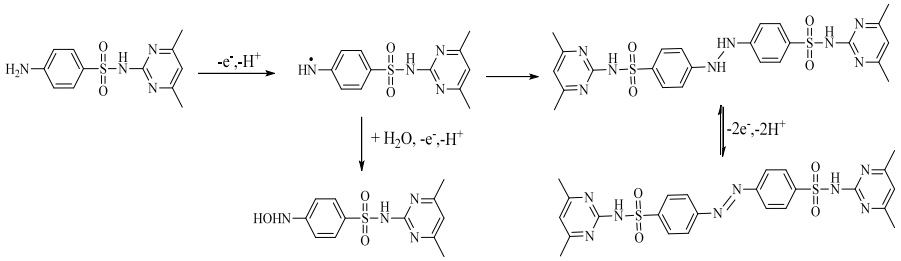


**3.7. Voltammetric Detection of SMZ.** Differential pulse voltammetry (DPV) was used to create an appropriate calibration curve for the detection of SMZ in 0.1 M of PBS (pH = 7.0) using the M-Chs-Aci/CPE. The parameters of DPV were optimized at a pulse amplitude of 25 mV, a pulse width of 50 ms, and a scan rate of 20 mV/s. The electrochemical response via the M-Chs-Aci/CPE is presented in Figure 9. The peak oxidative current increased remarkably linearly when the SMZ concentration increased from 0.08 to 6.0 M. Additionally, an obvious linear relationship between the concentration of SMZ (0.08 to 6.0 $\mu$M) and the peak of oxidative current was found, as illustrated in insets of Figure 9; the equation of such a linearity trend is provided by eq 8.

$$I_p\ (\mu A) = 9.36 + 5.84C\ (\mu M), \quad r^2 = 0.996 \tag{8}$$

using the following formulas: (LOD = 3 s/m) and (LOQ = 10 s/m), the LOD and LOQ were calculated to be 0.021 $\mu$M and 0.071 $\mu$M, respectively, where $S$ refers to the standard deviation of the peak current (3 cycles) of the linearity range at the minimum concentration and $m$ represents the slope of the calibration equation.[2] These results demonstrated the high sensitivity (5.84 $\mu$A/$\mu$M) of the new electrochemical sensor toward the SMZ oxidation. Variously adjusted electrodes were applied to compare the LOD for SMZ produced here, as shown in Table 1.

**3.8. Interference Study.** Common foreign species that may be present in real samples were successively added to 3.0 $\mu$M of SMZ test solution. The effect of the expected interferences on the anodic peak current of the SMZ was studied to determine the ability of the M-Chs-Aci/CPE for the precise detection of SMZ in the presence of different interferences or impurities, as shown in Table 1S. The tolerance limit was calculated to be less than 5.0% of the relative error (Table 2). The obtained results demonstrated that there is no significant influence on the SMZ anodic peak current in the presence of about a 350-fold excess of different inorganic ions like $K^+$, $Na^+$, $Ca^{2+}$, $Mg^{2+}$, $SO_4^{2-}$, $NO_3^-$, and $Cl^-$. Additionally, about 200-fold excess of some amino acids, such as glycine, methionine, and cysteine, as well as some organic materials, such as glucose, sucrose, and ascorbic acid. The calculated relative standard deviation (RSD) values were lower than 5%, proving the remarkable accuracy of this approach.

On the other hand, because other sulfa drugs (such as sulfamethoxazole and sulfanilamide) have comparable oxidation potentials, their presence could cause interference. Figure 10 displays the effect of different concentrations (0−3.0 $\mu$M) of sulfamethoxazole (A) and sulfanilamide (B) on the oxidation response of 3.0 $\mu$M SMZ at optimal conditions. It is clear that the presence of the sulfa drugs not only causes a broad potential peak for SMZ but also increases the anodic peak current with a relative error higher than 5.0%. While it is true that the selectivity of the M-Chs-Aci/CPE may not be


https://doi.org/10.1021/acsomega.3c10390
ACS Omega 2024, 9, 17323−17333

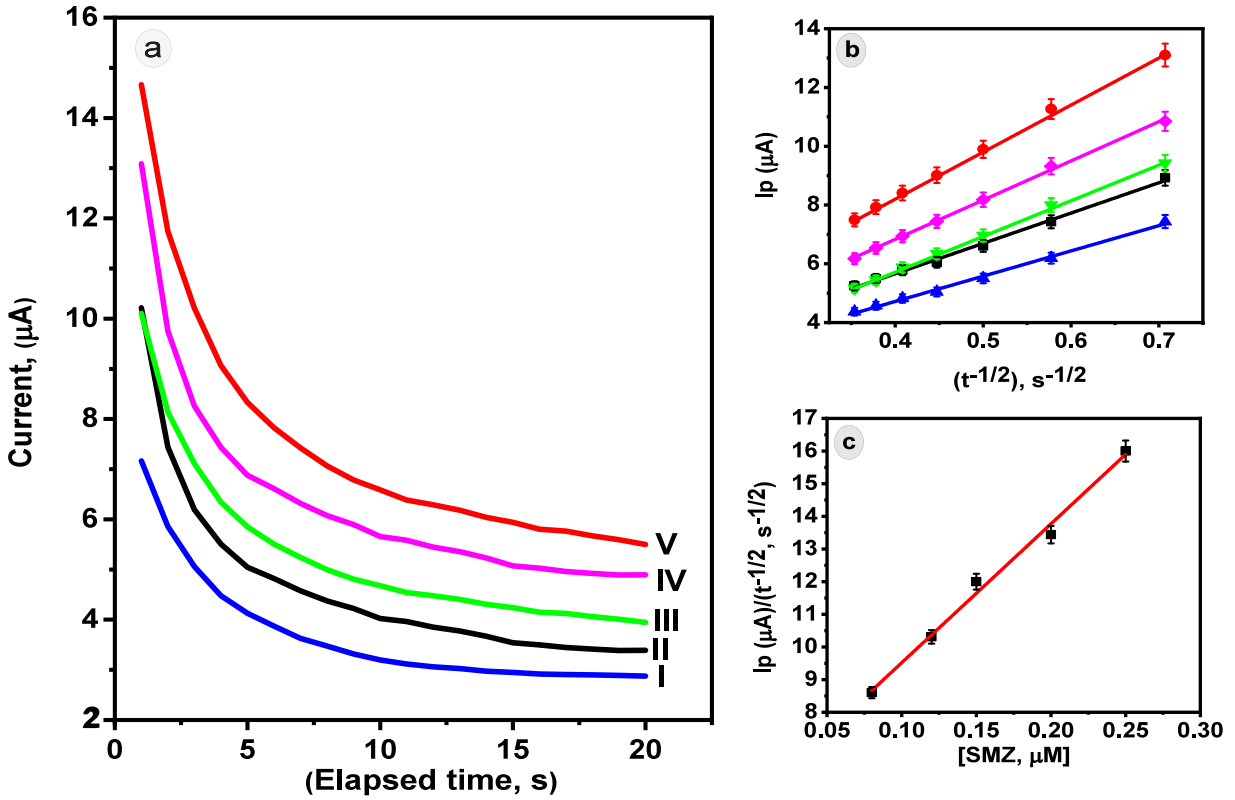


**Figure 8.** (a) Chronoamperograms of the M-Chs-Aci/CPE in 0.1 M PBS (pH = 7.0) comprising (I) 0.08 $\mu$M, (II) 0.12 $\mu$M, (III) 0.15 $\mu$M, (IV) 0.2 $\mu$M, and (V) 0.25 $\mu$M of SMZ. (b) Relationship between $I_p$ and the $t^{-0.5}$ obtained from the chronoamperogram measurements, and (c) the graph shows the slopes corresponding to the SMZ concentration

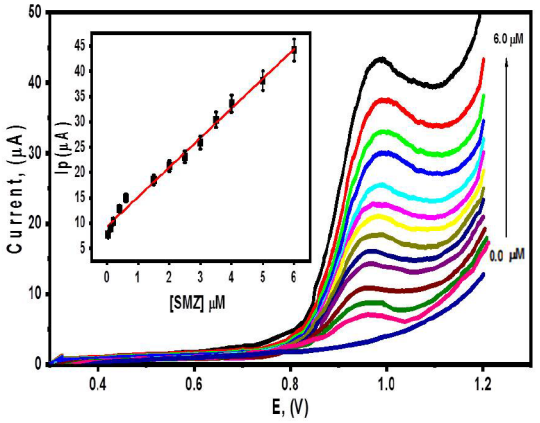


**Figure 9.** DPVs at the M-Chs-Aci/CPE for various SMZ concentrations (0.0–6.0 $\mu$M) in 0.1 M PBS (pH = 7.0). Pulse amplitude: 25 mV, pulse width: 50 ms, and scan rate: 20 mV/s. The inset part displays the calibration curve.

**Table 2. Tolerance Ratios of Foreign Species in the Determination of 3.0 $\mu$M SMZ in PBS (pH= 7.0)**

| foreign species | tolerance ratio ($C_{species}/C_{target\ analyte}$) |
|---|---|
| $K^+$, $Na^+$, $Ca^{2+}$, $Mg^{2+}$, $SO_4^{2-}$, $NO_3^-$, and $Cl^-$ | 350 |
| glycine, methionine, and cysteine | 200 |
| glucose, sucrose, and ascorbic acid | 200 |

exclusive to SMZ, it is important to note that no observable interference was detected in the SMZ oxidation peak. Therefore, one can conclude that the fabricated electrode exhibits high selectivity without any interfering influences on its analytical effectiveness. As a result, it can be considered an effective sensor for the detection of SMZ. However, it is acknowledged that further work is required to address the issue of selectivity and explore potential improvements in future studies.

**3.9. Repeatability, Reproducibility, and Stability.** The repeatability of the M-Chs-Aci/CPE was determined by

**Table 1. Comparison of the LOD for the Determination of the SMZ Using Various Modified Electrodes**

| method | working electrodes | linear ranges [$\mu$M] | LOD [$\mu$M] | references |
|---|---|---|---|---|
| DPASV | AgNP/TCBt/GCE | 0.89–107.7 | 0.097 | 2 |
| SWV | GO/Cu–Ag core–shell/GCE | 10–1000 | 0.46 | 14 |
| DPV | GC/rGO-AuNPs | 0.5–6.5 | 0.1 | 15 |
| Amperometry | i-t ($CeVO_4$/MWCNTs-GCE) | 0.1–113.4 | 0.02 | 16 |
| SWV | SPCE/PEDOT/$MnO_2$ | 1–500 | 0.16 | 43 |
| SWV | poly(3-methylthiophene)/GC | 0.9–500 | 0.37 | 44 |
| DPV | M-Chs-Aci/CPE | 0.08–6.0 | 0.021 | present work |



https://doi.org/10.1021/acsomega.3c10390
ACS Omega 2024, 9, 17323–17333

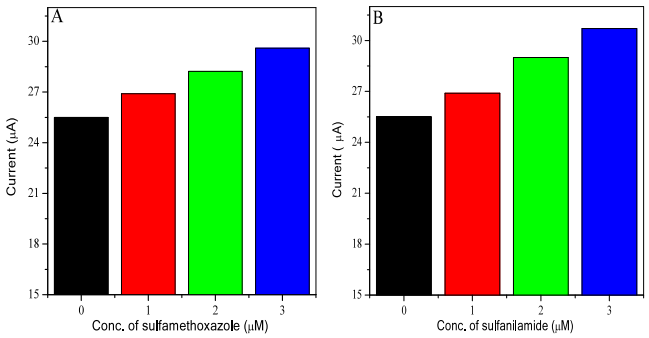


**Figure 10.** Effect of interferences on the detection of 3.0 $\mu$M SMZ in 0.1 M of PBS (pH 7.0), at the M-Chs-Aci/CPE in the presence of various concentrations (0, 1.0, 2.0, and 3.0 $\mu$M) of sulfamethoxazole (A) and sulfanilamide (B).

measuring the current signal change of 3.0 $\mu$M SMZ in six duplicates using DPV under the optimized conditions (Figure 2S). The obtained relative standard deviation (RSD) was 3.83%, which means the good repeatability of the modified electrode. Additionally, the reproducibility of the M-Chs-Aci/CPE was evaluated by successive measurements of 3.0 $\mu$M SMZ CPE in 0.1 M PBS (pH 7.0) using six equally fabricated electrodes, as can be seen in Figure 3S. The results indicated that the RSD of the peak current of the SMZ obtained on the six used electrodes was 3.31%. The electrochemical stability test of the M-Chs-Aci/CPE in 0.1 M PBS (pH 7.0) containing 3.0 $\mu$M SMZ was investigated by continuous CV measurements recorded at an interval of 7200 s in a day. The responses showed that the proposed M-Chs-Aci/CPE sensor decreases about 6.54% current response. Moreover, the long-term stability of the fabricated M-Chs-Aci/CPE was estimated as shown in Figure 4S. Based on the obtained results, after 21 days of storage at ambient temperature (25 °C), the M-Chs-Aci/CPE retains 94.87% of its initial response. Consequently, the proposed sensor M-Chs-Aci/CPE displayed acceptable repeatability, reproducibility, and stability.

**3.10. DPV Detection of SMZ in the Milk Sample.** The voltammetric sensing efficiency of the prepared M-Chs-Aci/CPE for the detection of SMZ in the milk sample was investigated using the conventional addition method. DPV measurements of SMZ at the M-Chs-Aci/CPE in the milk sample under optimal conditions displayed appropriate accuracy with recoveries ranging from 95.0% to 98.87%, as illustrated in Table 2. As a result of these findings, the proposed M-Chs-Aci/CPE demonstrates an effective potential for the detection of SMZ in real samples (Table 3).

## 4. CONCLUSIONS

A simple, novel, and economical development of a Magnetite-Chs-Aci nanocomposite was utilized for further enhancement of the electrocatalytic activity of the CPE. The prepared M-Chs-Aci nanocomposite was characterized by techniques, including FT-IR, XRD, EDX, SEM, and TEM. The fabricated M-Chs-Aci/CPE demonstrated more compatible electrocatalytic performance toward the $[Fe(CN_6)]^{3-/4-}$redox couple compared with the bare BCPE. Remarkably, the electroactive surface area of the modified electrode increased by (0.034 $cm^2$) compared with that of the BCPE. Furthermore, the M-Chs-Aci/CPE displayed excellent electrocatalytic efficiency toward the SMZ oxidation in 0.1 M of PBS (pH 7.0). In addition, the anodic current signal of the SMZ revealed a linear dependence on the SMZ concentration from 0.08 to 6.0 $\mu$M and the values of LOD and LOQ were evaluated at 0.021 $\mu$M and 0.071 $\mu$M, respectively. The nanocomposite also attained a high diffusion coefficient value and good repeatability, recorded at 9.4 x $10^{-6}cm^2/s$ and 3.83%, respectively. Moreover, the modified electrode retained approximately 94.87% of its initial response after 21 days. Finally, the proposed M-Chs-Aci/CPE was employed for the SMZ detection in milk samples with acceptable recoveries ranging from 95%−98.87%. These results confirm that the M-Chs-Aci/CPE is a promising sensor, opening new frontiers in the determination of SMZ in real samples.

**Table 3. Detection of SMZ in Milk Samples Using the M-Chs-Aci/CPE**

| samples | SMZ added ($\mu$M) | SMZ found ($\mu$M) | recovery % |
|---|---|---|---|
| milk | 5 | 4.75 | 95.0 |
| | 10 | 9.86 | 98.60 |
| | 15 | 14.83 | 98.87 |

## ■ ASSOCIATED CONTENT

### Data Availability Statement

Data will be made available on request.

### Supporting Information

The Supporting Information is available free of charge at https://pubs.acs.org/doi/10.1021/acsomega.3c10390.

Discussion the effect of M-Chs-Aci content in the paste on the peak current of SMZ; influence of the M-Chs-Aci content in CPE on the current response of SMZ (Figure 1S); six DPV duplicates of (3.0 $\mu$M) SMZ at M-Chs-Aci/CPE in 0.1 M of PBS (pH = 7.0) (Figure 2S); DPVs of (3.0 $\mu$M) SMZ at six reproducible M-Chs-Aci/CPE in 0.1 M of PBS (pH = 7.0) (Figure 3S); DPV of (3.0 $\mu$M) SMZ at M-Chs-Aci/CPE in 0.1 M of PBS (pH = 7.0) after different days (Figure 4S); interference effects on the determination of 3.0 $\mu$M SMZ in 0.1 M PBS (pH= 7.0) (Table 1S) (PDF)

## ■ AUTHOR INFORMATION

### Corresponding Author

**Mohamed Abd-Elsabour** − *Chemistry Department, Faculty of Science, Luxor University, Luxor 85951, Egypt*; Email: m.sabour28@sci.svu.edu.eg

### Authors

**Mortaga M. Abou-Krisha** − *Chemistry Department, College of Science, Imam Mohammad Ibn Saud Islamic University (IMSIU), Riyadh 11623, Saudi Arabia; Chemistry Department, Faculty of Science, South Valley University, Luxor 85951, Egypt*

**Abdulrahman G. Alhamzani** − *Chemistry Department, College of Science, Imam Mohammad Ibn Saud Islamic University (IMSIU), Riyadh 11623, Saudi Arabia*

**Abdullah N. Alotaibi** − *Chemistry Department, College of Science, Imam Mohammad Ibn Saud Islamic University (IMSIU), Riyadh 11623, Saudi Arabia*

**Tarek A. Yousef** − *Chemistry Department, College of Science, Imam Mohammad Ibn Saud Islamic University (IMSIU), Riyadh 11623, Saudi Arabia; Department of Toxic and*



https://doi.org/10.1021/acsomega.3c10390
ACS Omega 2024, 9, 17323−17333

*Narcotic Drug, Forensic Medicine, Mansoura Laboratory, Medicolegal Organization, Cairo 11435, Egypt*

Complete contact information is available at: https://pubs.acs.org/10.1021/acsomega.3c10390

### Author Contributions

M.A.-E., A.G.A., and .N.A.: Supervision, writing—review and editing. M.A.-E., Ta.A.Y., and M.M.Ab.-K.: Conceptualization, methodology, investigation, data curation, writing—review and editing. All authors have read and agreed to the published version of the manuscript.

### Notes

The authors declare no competing financial interest.

## ■ ACKNOWLEDGMENTS

The authors extend their appreciation to the Deputyship for Research & Innovation, Ministry of Education in Saudi Arabia for funding this research through the project number IFP-IMSIU-2023096. The authors also appreciate the Deanship of Scientific Research at Imam Mohammad Ibn Saud Islamic University (IMSIU) for supporting and supervising this project.

## ■ REFERENCES

(1) de Zayas-Blanco, F.; García-Falcón, M. S.; Simal-Gándara, J. Determination of sulfamethazine in milk by solid phase extraction and liquid chromatographic separation with ultraviolet detection. *Food Control* **2004**, *15*, 375−378.

(2) Lalmalsawmi, J.; Tiwari, D.; Lee, S. M.; Kim, D. J.; Kim, H. Efficient electrochemical sensor for trace detection of sulfamethazine in spring water: Use of novel nanocomposite material coated with Ag or Au nanoparticles. *Microchem. J.* **2022**, *179*, 107520.

(3) Bai, X.; You, T.; Sun, H.; Yang, X.; Wang, E. Determination of three *β*-blockers by capillary electrophoresis with end-column electrochemical detection. *Electroanalysis* **2000**, *12*, 1379−1382.

(4) Qing-Cui, C.; Xiu-Hui, T.; Lian-Mei, J.; Wen-Jun, Z.; Jian-Nong, Y. Determination of Effective Ingredients in Compound Sulfamethoxazole Tablets by Capillary Electrophoresis with Amperometric Detection. *Chin. J. Anal. Chem.* **2008**, *36*, 292−296.

(5) Gu, G. Z.; Xia, H. M.; Pang, Z. Q.; Liu, Z. Y.; Jiang, X. G.; Chen, J. Determination of sulphasalazine and its main metabolite sulphapyridine and 5-aminosalicylic acid in human plasma by liquid chromatography/tandem mass spectrometry and its application to a pharmacokinetic study. *J. Chromatogr. B: Anal. Technol. Biomed. Life Sci.* **2011**, *879*, 449−456.

(6) Teshima, D.; Hino, B.; Itoh, Y.; Oishi, R. Simple and simultaneous determination of sulphapyridine and acetylsulphapyridine in human serum by column-switching high-performance liquid chromatography. *J. Clin. Pharm. Ther.* **2002**, *27*, 403−408.

(7) Preechaworapun, A.; Chuanuwatanakul, S.; Einaga, Y.; Grudpan, K.; Motomizu, S.; Chailapakul, O. Electroanalysis of sulfonamides by flow injection system/high-performance liquid chromatography coupled with amperometric detection using boron-doped diamond electrode. *Talanta* **2006**, *68* (5), 1726−1731.

(8) Koesukwiwat, U.; Jayanta, S.; Leepipatpiboon, N. Validation of a liquid chromatography-mass spectrometry multi-residue method for the simultaneous determination of sulfonamides, tetracyclines, and pyrimethamine in milk. *J. Chromatogr. A* **2007**, *1140*, 147−156.

(9) Assassi, N.; Tazerouti, A.; Canselier, J. P. Analysis of chlorinated, sulfochlorinated and sulfonamide derivatives of n-tetradecane by gas chromatography/mass spectrometry. *J. Chromatogr. A* **2005**, *1071*, 71−80.

(10) Chen, S. H.; Li, Y. X.; Li, P. H.; Xiao, X. Y.; Jiang, M.; Li, S. S.; Zhou, W. Y.; Yang, M.; Huang, X. J.; Liu, W. Q. Electrochemical spectral methods for trace detection of heavy metals: A review. *TrAC, Trends Anal. Chem.* **2018**, *106*, 139−150.

(11) Singh, B.; Bhat, A.; Dutta, L.; Pati, K. R.; Korpan, Y.; Dahiya, I. Electrochemical Biosensors for the Detection of Antibiotics in Milk: Recent Trends and Future Perspectives. *Biosensors* **2023**, *13*, 867.

(12) Liu, R.; Zhang, X.; Zhang, C.; Deng, X.; Wu, T.; Liu, R.; Sun, Y. A novel Ag/g-$C_3N_4$/GCE sensor for highly efficient electrochemical detection of sulfamethoxazole. *J. Phys. Conf. Ser.* **2024**, *2680* (1), 6−12.

(13) He, B.; Li, M.; Li, M. Electrochemical determination of sulfamethazine using a gold electrode modified with multi-walled carbon nanotubes, graphene oxide nanoribbons and branched aptamers. *Microchim. Acta* **2020**, *187*, 274.

(14) Feizollahi, A.; Rafati, A. A.; Assari, P.; Joghani, R. A. Development of an electrochemical sensor for the determination of antibiotic sulfamethazine in cow milk using graphene oxide decorated with Cu−Ag core−shell nanoparticles. *Anal. Methods* **2021**, *13* (7), 910−917.

(15) Silva, M.; Cesarino, I. Evaluation of a nanocomposite based on reduced graphene oxide and gold nanoparticles as an electrochemical platform for detection of sulfamethazine. *J. Compos. Sci.* **2019**, *3* (2), 1−12.

(16) Nataraj, N.; Chen, S.-M. Interfacial Influence of Strontium Niobium Engulfed Reduced Graphene Oxide Composite for Sulfamethazine Detection: Employing an Electrochemical Route in Real Samples. *J. Electrochem. Soc.* **2021**, *168*, 057512.

(17) Govindaraj, M.; Rajendran, J.; P K, U. G.; Muthukumaran, M. K.; Jayaraman, B.; J, A. S. Graphitic Carbon Nitride Nanosheets Decorated with Strontium Tungstate Nanospheres as an Electrochemical Transducer for Sulfamethazine Sensing. *ACS Appl. Nano Mater.* **2023**, *6* (2), 930−945.

(18) Ma, J.; Zhang, C.; Hong, X.; Liu, J. Incorporating Cerium Vanadate into Multi-Walled Carbon Nanotubes for Fabrication of Sensitive Electrochemical Sensors toward Sulfamethazine Determination in Water Samples. *Chemosensors* **2023**, *11*, 64.

(19) Soni, I.; Kumar, P.; Sharma, S.; Jayaprakash, G. K. A Short Review on Electrochemical Sensing of Commercial Dyes in Real Samples Using Carbon Paste Electrodes. *Electrochem* **2021**, *2* (2), 274−294.

(20) Palanna, M.; Mohammed, I.; Aralekallu, S.; Nemakal, M.; Sannegowda, L. K. Simultaneous detection of paracetamol and 4-aminophenol at nanomolar levels using biocompatible cysteine-substituted phthalocyanine. *New J. Chem.* **2020**, *44*, 1294−1306.

(21) Sainz-Urruela, C.; Vera-López, S.; San Andrés, M. P. S.; Díez-Pascual, A. M. Graphene-based sensors for the detection of bioactive compounds: A review. *Int. J. Mol. Sci.* **2021**, *22* (7), 3316.

(22) Morin-Crini, N.; Lichtfouse, E.; Torri, G.; Crini, G. Applications of chitosan in food, pharmaceuticals, medicine, cosmetics, agriculture, textiles, pulp and paper, biotechnology, and environmental chemistry. *Environ. Chem. Lett.* **2019**, *17*, 1667−1692.

(23) Dong, Y.; Bi, J.; Ming, S.; Zhang, S.; Zhu, D.; Meng, D.; Li, T. Functionalized chitosan as a novel support for stabilizing palladium in Suzuki reactions. *Carbohydr. Polym.* **2021**, *260*, 117815.

(24) Annu, R.; N, A. Recent development in chitosan-based electrochemical sensors and its sensing application. *Int. J. Biol. Macromol.* **2020**, *164*, 4231−4244.

(25) Zouaoui, F.; Bourouina-Bacha, S.; Bourouina, M.; Jaffrezic-Renault, N.; Zine, N.; Errachid, A. Electrochemical sensors based on molecularly imprinted chitosan: A review. *TrAC, Trends Anal. Chem.* **2020**, *130*, 115982.

(26) Peng, X.; Dong, K.; Zhang, Y.; Wang, L.; Wei, C.; Lv, T.; Wang, Z. L.; Wu, Z. Sweat-Permeable, Biodegradable, Transparent and Self-powered Chitosan-Based Electronic Skin with Ultrathin Elastic Gold Nanofibers. *Adv. Funct. Mater.* **2022**, *32*, 1−10.

(27) Chauhan, S.; Thakur, A. Chitosan-Based Biosensors-A Comprehensive Review. *Mater. Today: Proc.* **2023**. .

(28) Deng, P.; Zhou, C.; Wei, Y.; Yue, X.; Li, J.; Yao, L.; Ding, J.; He, Q. Salicylaldehyde functionalized chitosan for electrochemical sensitive sensor: Simultaneous determination of catechol and hydroquinone. *J. Electroanal. Chem.* **2022**, *918*, 116506.

(29) El-Naggar, M. M.; Haneen, D. S. A.; Mehany, A. B. M.; Khalil, M. T. New synthetic chitosan hybrids bearing some heterocyclic moieties with potential activity as anticancer and apoptosis inducers. *Int. J. Biol. Macromol.* **2020**, *150*, 1323−1330.
(30) Baghayeri, M.; Veisi, H.; Farhadi, S.; Beitollahi, H.; Maleki, B. Ag nanoparticles decorated $Fe_3O_4$/chitosan nanocomposite: Synthesis, characterization and application toward electrochemical sensing of hydrogen peroxide. *J. Iran. Chem. Soc.* **2018**, *15*, 1015−1022.
(31) Nemakal, M.; Shantharaja, G.; Sannegowda, M.; Palanna, L. K.; Kumar, P. S.; Sharath Kumar, P. Zinc phthalocyanine anchored magnetite particles: Efficient platform for sensing of thiocyanate. *J. Electroanal. Chem.* **2021**, *895*, 115385.
(32) Freire, T. M.; Dutra, L. M. U.; Queiroz, D. C.; Ricardo, N. M. P. S.; Barreto, K.; Denardin, J. C.; Wurm, F. R.; Sousa, C. P.; Correia, A. N.; De Lima-Neto, P.; Fechine, P. B. A. Fast ultrasound assisted synthesis of chitosan-based magnetite nanocomposites as a modified electrode sensor. *Carbohydr. Polym.* **2016**, *151*, 760−769.
(33) Anicuta, S.; Dobre, L.; Stroescu, M.; Jipa, I. Fourier transform infrared (ftir) spectroscopy for characterization of antimicrobial films containing chitosan. *An. Univ. Oradea, Fasc.: Ecotoxicologie, Zooteh. Si Tehnologii de Ind. Alimentară*. **2010**, 12341240.
(34) Arjunan, V.; Durgadevi, G.; Mohan, S. An experimental and theoretical investigation on the structure, vibrations and reactivity properties of pharmacologically active compounds 3−acetylindole and indole−3−acetamide. *J. Mol. Struct.* **2020**, *1210*, 128012.
(35) Jiao, T. F.; Zhou, J.; Zhou, J. X.; LiHua, G.; Xing, Y. Y.; Li, X. H. Synthesis and characterization of chitosan-based schiff base compounds with aromatic substituent groups. *Iran. Polym. J.* **2011**, *20*, 123−136.
(36) Dung, D. T. K.; Hai, T. H.; Phuc, L. H.; Long, B. D.; Vinh, L. K.; Truc, P. N. Preparation and characterization of magnetic nanoparticles with chitosan coating. *J. Phys. Conf. Ser.* **2009**, *187*, 012036.
(37) Madian, N. G.; Mohamed, N. Enhancement of the dynamic mechanical properties of chitosan thin films by crosslinking with greenly synthesized silver nanoparticles. *J. Mater. Res. Technol.* **2020**, *9*, 12970−12975.
(38) Jaafari, J.; Barzanouni, H.; Mazloomi, S.; Farahani, N. A. A.; Sharafi, K.; Soleimani, P.; Haghighat, G. A. Effective adsorptive removal of reactive dyes by magnetic chitosan nanoparticles: Kinetic, isothermal studies and response surface methodology. *Int. J. Biol. Macromol.* **2020**, *164*, 344−355.
(39) Atangana, E.; Chiweshe, T. T.; Roberts, H. Modification of Novel Chitosan-Starch Cross-Linked Derivatives Polymers: Synthesis and Characterization. *J. Polym. Environ.* **2019**, *27*, 979−995.
(40) Abd-Elsabour, M.; Abou-Krisha, M. M.; Kenawy, S. H.; Yousef, T. A. A Novel Electrochemical Sensor Based on an Environmentally Friendly Synthesis of Magnetic Chitosan Nanocomposite Carbon Paste Electrode for the Determination of Diclofenac to Control Inflammation. *Nanomaterials* **2023**, *13*, 1079.
(41) Mutharani, B.; Chen, T. W.; Chen, S. M.; Liu, X. Reversibly switchable ruthenium hybrid thermo-responsive electrocatalyst-based voltammetric sensor for sensitive detection of sulfamethazine in milk samples. *Sens. Actuators, B* **2020**, *316*, 128103.
(42) Mostafazadeh, R.; Karimi, H.; Ghaffarinejad, A.; Tajabadi, F.; Hamidian, Y. Highly sensitive electrochemical sensor based on carbon paste electrode modified with graphene nanoribbon−CoFe2O4@ NiO and ionic liquid for azithromycin antibiotic monitoring in biological and pharmaceutical samples. *Appl. Nanosci.* **2023**, *13* (9), 5829−5838.
(43) Su, Y. L.; Cheng, S. H. A novel electroanalytical assay for sulfamethazine determination in food samples based on conducting polymer nanocomposite-modified electrodes. *Talanta* **2018**, *180*, 81−89.
(44) Msagati, T. A. M.; Ngila, J. C. Voltammetric detection of sulfonamides at a poly(3-methylthiophene) electrode. *Talanta* **2002**, *58*, 605−610.



https://doi.org/10.1021/acsomega.3c10390
*ACS Omega* 2024, 9, 17323−17333